High Temperature. Vol. 43, No. 1, 2005, pp. 141–150. Translated from Teplofizika Vysokikh Temperatur, Vol. 43, No. 1, 2005, pp. 136–145.

REVIEW

Measurements of the Viscosity of Water under Shock Compression

V. N. Mineev and A. I. Funtikov

Institute of High Energy Densities, Joint Institute of High Temperatures, Russian Academy of Sciences (IVTAN), Moscow, 125412 Russia

Received April 23, 2004

Abstract—The results of measurements of the shear viscosity of shock-loaded water, obtained by the method of decay of perturbations on a corrugated shock front suggested by Sakharov *et al.* [1], are treated in the light of new data on the phase diagram of water. The experimental data on viscosity in the pressure range from 4 to 25 GPa are compared to the results of measurements by other methods. The high values of viscosity at high pressures are attributed to the formation a water-ice VII mixture under shock compression of water.

INTRODUCTION

The properties of water and ice at high pressures and temperatures are investigated for the purpose of studying the physics of condensed state of matter, physical chemistry, geophysics, planetology, and the most diverse problems in science and engineering. At relatively low pressures (less than 1 GPa), the rheological properties of water, including viscosity, are essential for the investigation of hydrodynamic and heattransfer processes. At present, the reological properties of water are used in designing power plants of some types, as well as in developing new technologies in the food industry [2] and medicine where, in particular, the shock compression of water has come to be used for lithotripsy [3].

No unambiguous account of the behavior of viscosity of water was obtained at higher pressures attained as a result of shock compression [4]. The available data obtained using different methods of measurement are at variance with one another [5–10].

Singular features of water, which are associated with its phase diagram and distinguish its properties from the behavior of simple liquids, show up in both ranges of pressure.

Bridgman [11] was the first to measure the viscosity of water to pressures up to 1.1 GPa in the temperature range from zero to 75 °C. Later on, fairly well coinciding results in this pressure range were obtained in [2, 12–14] using different procedures. It was found that, on the isotherms $T = -10$ to $+20$ °C, the viscosity has a minimum in the pressure range $P < 0.2$ GPa where the melting curve for ice I is located with an anomalous slope $dT/dP < 0$ (Fig. 1). In the opinion of DeFries, Jonas, and Wilbur [13, 14], the decrease in viscosity with increasing pressure is associated with the transformation of hydrogen bonds; this, in turn, causes the variation of size and disintegration of some part of clusters which exist in water under normal conditions and enable one to treat this water as a state of "water in water" [2, 15]. When the temperature

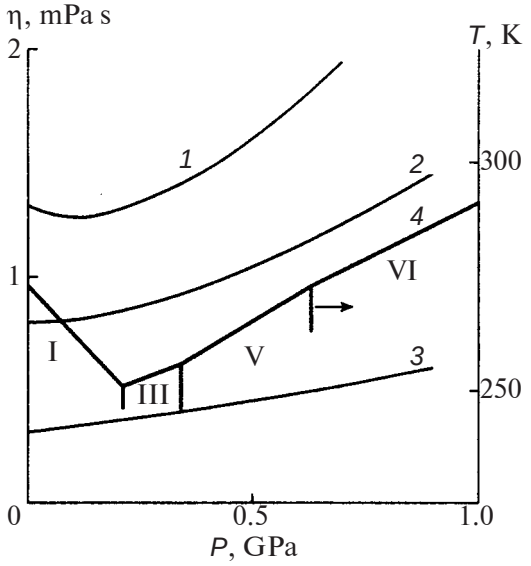

Fig. 1. Variation of the viscosity of water on isotherms: (*1–3*) isotherms T = 283, 303, and 363 K; (*4*) position of the water–ice interface on the T–P diagram.

0018-151X/05/4301-0141

increases, $T > 20$°C, and in the pressure range $P > 0.2$ GPa, an increase in viscosity with increasing pressure on the isotherms occurs in the entire pressure range.

The diagram of viscosity of water for initial states on the melting curve was analyzed by Lyusternik [16]. In contrast to simple liquids, the viscosity varies nonmonotonically in the region contiguous to the phases of ice I, III, V, and VI. The viscosity increases from the initial value of $\eta_0 = 1.8$ mPa s at $P = 0.1$ MPa and $T = 293$ K up to the triple point ice I–ice III by a factor of almost three to $\eta = 4.6$ mPa s, and then decreases gradually to the triple point ice VI–ice VII at which the value of viscosity is minimal. Then, the viscosity increases with pressure. The variation of viscosity on this branch of the curve of solidification of water issuing from the triple point ice VI–ice VII with the parameters $P = 2.2$ GPa, $T = 355$ K, $\rho_w = 1.33$ g/cm^3, and $\eta = 1.4$ mPa s was calculated by Lyusternik [16] using model quasi-gas concepts for the Enskog hard spheres [17]. The variation of viscosity correlates with that of density and corresponds to the behavior of classical liquid. According to the estimates of Lyusternik [16], at $T = 870$ K and $\rho_w = 1.8$ g/cm^3, the viscosity increases to $\eta = 5$ mPa s.

The compression of matter by means of shock waves [18] makes it possible to attain higher pressures inaccessible by static methods. However, the parameters of compressed matter, in particular, viscosity, are defined by the processes which accompany the shock compression, namely, high-rate strain on the shock front, nonadiabatic heating, and the flow of matter behind the shock front. In so doing, the viscosity shows up both in the effect on the width of the shock front and in the dissipative processes which accompany the shock wave propagation.

The methods employed to determine the viscosity of water using shock waves include the development of preassigned harmonic perturbations on the shock front [1, 5, 6] and the measurements of the velocity of a cylindrical body arranged along the shock front and being involved in motion [7–9] and of the impurity electrical conductivity of weak aqueous solutions [10, 19]. The maximal values of shock-compression pressure (up to 25 GPa) were obtained in [5, 6]. The shock compression of water made obvious the singular features of its phase diagram and the possibility of freezing, i.e., transition of water into the state of ice VII with increasing pressure [3, 20–23].

SHOCK ADIABATIC CURVE OF WATER

Systematic investigations of shock compression of water were started in the 1950s by Walsh and Rice [20] and Al'tshuler, Bakanova, and Trunin [21]. The range of pressures varied from up to 25 GPa in [20] to up to 80 GPa in [21]. Later on, these results were refined largely to pressures of ~100 GPa [24–28]. The measurement results were represented in the form of the dependence of the shock wave velocity D on the mass velocity U of matter behind the shock front. These data are used, along with the laws of conservation of mass and momentum, to determine the pressure and compression ratio $\sigma = \rho/\rho_0$ (ρ and ρ_0 denote the density of compressed and initial matter, respectively),

$$P = \rho_0 UD; \quad \sigma = D/(D - U). \qquad (1)$$

Even in the first measurements [21, 22], it was found that the shock adiabatic curve of water from the initial state at $T_0 = 20$ °C in the D–U coordinates in the pressure range of ~12–13 GPa had an inflection which was attributed to the crossing of the shock adiabatic curve by the melting curve of ice. Walsh and Rice [20] attributed this effect to analogy with melting of ice I on the shock adiabatic curve from the initial state at $T_0 = -10$ °C. It was further assumed that the first intersection of the shock adiabatic curve of water with the melting curve, which is responsible for the formation of ice VII behind the shock front, may occur in the region of lower pressures. However, no corresponding inflection was observed on the $D(U)$ curves. Therefore, these dependences were represented in [22, 27–30] by two linear segments of different slopes, the position of whose inflections corresponded to their intersection.

Further processing of experimental results in [31, 32] made it possible to approximate the shock adiabatic curve of water by three linear segments for which the correlations and limits of validity were found by successive fitting of values of $D(U)$ from the total array of experimental data. The dependences obtained in [32] are given in Fig. 2. The first inflection on the discontinuity of the $D(U)$ curve corresponded to a pressure of 2.1–2.3 GPa, and the second inflection – to 10.5–12.2 GPa.

A better impression of the shock adiabatic curve in the pressure range $P < 2$ GPa was obtained by Nagayama *et al.* [3] who produced a shock compression of water by an impact of a polymer plate at a velocity of

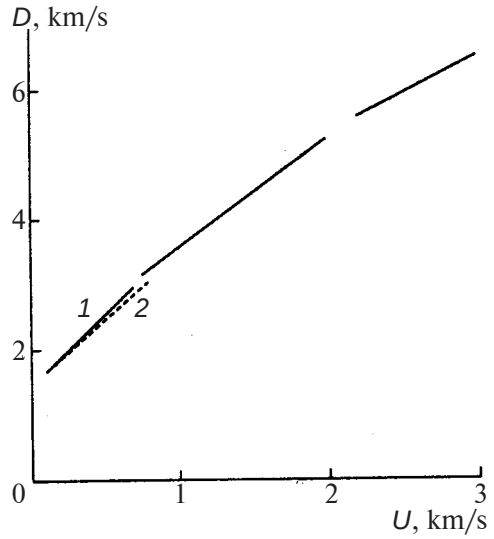

Fig. 2. *D–U* dependences for the adiabatic curve of shock compression of water: (*1*) data of [32], (*2*) data of [3].

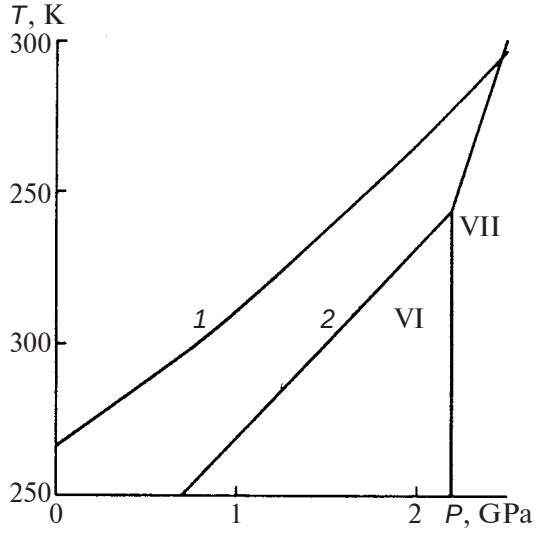

Fig. 3. The phase diagram for water in the region of ice VI and VII: (*1*) shock adiabatic curve for water [3], (*2*) interface [16].

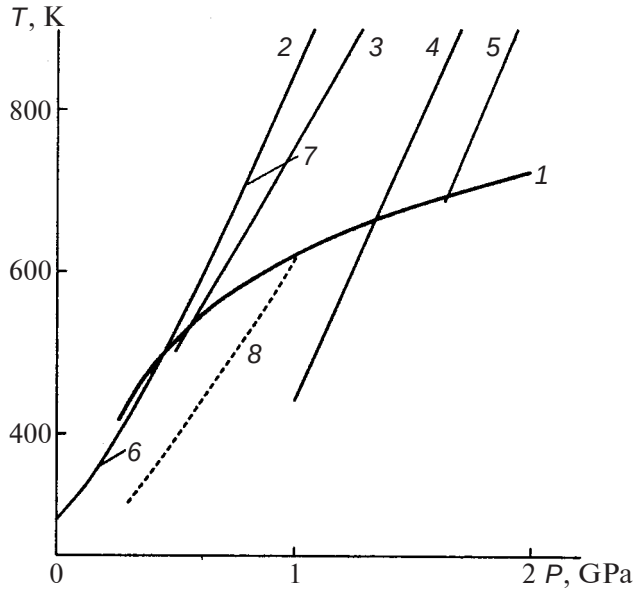

Fig. 4. The melting curve and shock adiabatic curves for water: (*1*) melting curve, (*2–5*) shock adiabatic curves: (*2*) data of [35], (*3*) data of [38], (*4*) data of [29], (*5*) data of [32], (*6*, *7*) double-compression shock adiabatic curves [34], (*8*) shock adiabatic curve for water–ice VII mixture [32].

less than 500 m/s. The position of the shock adiabatic curve calculated by the equation of state and of the melting curve in the *T–P* phase diagram is shown in Fig. 3. The intersection of he shock adiabatic curve with the melting curve according to the data of [31, 32] is fairly close to the value of pressure P_1 = = 2.4 GPa obtained by Nagayama *et al.* [3].

The possibility of formation of ice VII was the subject of study in the experiments of [20–23, 33, 34] which involved optical sounding of the state of matter behind the shock front. It turned out that, except for the results of Al'tshuler *et al.* [21] which were not confirmed by other researchers, no variation of transparency of shock-compressed water was observed in the pressure range from 3 to 30 GPa. At the same time, the shock adiabatic curve of water in the *T–P* phase diagram, calculated by the equation of state [35], as was shown in [34], almost contacted the melting curve for ice [36] in the vicinity of ~4 GPa. Therefore, double compression of water was necessary to get into the region of existence of ice VII. The experimental results of Kormer, Yushko, and Krishkevich [23, 34] were treated as being indicative of the formation of fine crystalline ice behind the front of the second shock wave. The time of ice formation was estimated at 10^{-6}–10^{-7} s. However, the obtained data could not be used to judge the completeness of phase transition under such conditions. When the pressure in the first shock wave was increased, P > 12–15 GPa, states were obtained which *a priori* corresponded to the liquid phase.

Figure 4 gives the phase diagram and calculated shock adiabatic curves for water, which correspond to the region of states above the melting curve. Also given in this figure are adiabatic curves of double com-

pression of water [34]. The melting curve for ice VII is based on the refined results of Fei *et al.* [37] up to a pressure P = 20 GPa. Preliminary estimates of pressure P_2 at the point of intersection of the melting curve and shock adiabatic curves issuing from the region of higher pressures [29, 35, 38] were obtained in [32, 34] by the data of previous measurements of melting curves for ice VII [36, 39] at somewhat lower temperatures than in the data of [37]. One can see in Fig. 4 that the values of P_2 on the shock adiabatic curves are as follows: curve *2* – 5.2 [35], curve *3* – 6.5 [38], and curve *4* – 13.5 GPa [29].

All of the calculated shock adiabatic curves for water in the *T*–*P* diagram corresponded to equations of state for the liquid phase. The equation of state in the Mie–Grüneisen form was obtained by Rice and Walsh [35] using the experimental data on shock compressibility [20]. The values of temperature of shock compression for water, obtained by the equations of state of [40], turned out to be fairly close to the results of [35].

The temperature of shock-compressed water was measured at a pressure of 30–40 GPa by Kormer [34], and then at a pressure of 50–80 GPa by Lyzenga *et al*. [41]. The values of temperature calculated in [35, 40] turned out to be overestimated by approximately 10% compared to the results of temperature measurements by Kormer [34]. An even more significant difference between the data of [35, 40] and [41] was revealed. The equation of state refined in [38], which included the temperature dependence of heat capacity C_V (in [35] the heat capacity was taken to be constant), turned out to be closer to both the experimental data of [34] and the data of [41]. At the same time, the values of temperature on the shock adiabatic curve, obtained as a result of quantum-mechanical calculation of the interaction potential of water molecule [42], turned out to be significantly overestimated (by approximately 500 K) compared to the measurement data of [34, 41].

Bakanova *et al.* [29] derived the equation of state for water using the experimental data on the shock compressibility of water at T_0 = 20 °C and of samples of ice and pressed snow from the state at T_0 = –15 °C with a normal and artificially reduced initial density. The value of the Grüneisen coefficient was determined in the approximation of free volume theory. The calculated values of temperature on the shock adiabatic curve for water turned out to be approximately 5% lower than the results of [34].

Zharkov and Trubitsyn [43] reviewed the data on wide-range interpolation equations of state for water and made comparison of the corresponding zero isotherms.

The transition to the region of solidification of water under shock compression (Fig. 4) must result in the formation of nuclei, i.e., crystal microdomains, in water. In addition to these nuclei, noncrystal structures may arise in the vicinity of the solidification point, such as clusters containing a number of particles which exhibit thermodynamic parameters close to those of crystal nuclei [44]. Structures of both types must be located within a more disordered and less dense liquid. The possibility of the formation of such clusters in water was indicated in [30, 45]. Precrystallization effects in liquids show up first of all as an anomalous increase in viscosity [44].

In a two-phase region, the weight fraction α of ice being formed on the shock adiabatic curve for the mixture of ice VII and water is calculated in accordance with the additive contribution of components at equilibrium pressure and temperature. The specific volume V of the mixture and the internal energy E are

$$\begin{aligned} V &= \alpha V_1 + (1 - \alpha) V_2, \\ E &= \alpha E_1 + (1 - \alpha) E_2, \end{aligned} \qquad (2)$$

where the subscripts 1 and 2 indicate the components of the mixture, i.e., ice VII and water, respectively.

Rybakov and Rybakov [32] used the Mie–Grüneisen coefficient to estimate α in the approximation of constant values of heat capacity C_V and Grüneisen coefficient γ equal for the components, as well as of the same isotherm $P_x(V)$, at T_0 = 300 K. In this case, the pressure of two-phase mixture is

$$P = P_x + \gamma(T - T_0)\frac{(\alpha C_{V1} + (1 - \alpha) C_{V2})}{V}. \qquad (3)$$

The $P_x(V)$ curve agreed with the experimental data for the isotherm T = 300 K of ice VII in the range from 3 to 8 GPa [46][1]. The melting heat determined from the Clausius–Clapeyron relation was taken into account in the equation for energy (2) on the melting curve.

[1]The isotherm T = 300 K of ice VII was later determined up to a pressure of 128 GPa in [47] and, in more detail, up to a pressure of 20 GPa in [37].

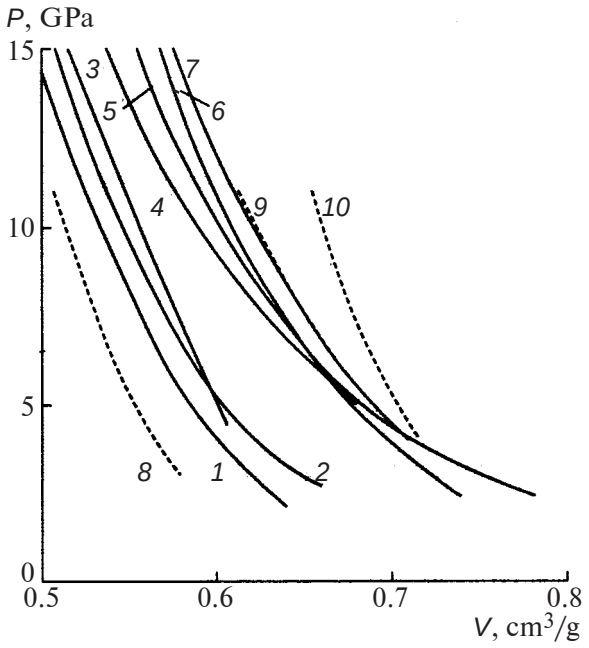

Fig. 5. *P–V* diagram for water. Solid curves: (*1*, *2*) isotherms T = 300 and 600 K for ice VII [37], (*3*) $P(V)$ on the melting curve for ice VII [37], (*4*) isotherm T = 573 K for water [49], (*5*) isentrope for water (T = 340–440 K) [28], (*6*) shock adiabatic curve for water [35], (*7*) shock adiabatic curve for water [29]. Dotted curves – shock adiabatic curves [32]: (*8*) for ice VII, (*9*) for two-phase mixture, (*10*) for water.

The pressure P_2 at the point of intersection of the adiabatic curve from the region of liquid phase of water [32] with the melting curve of [36] was 16.4 GPa. This value turned out to be close to the estimates made in [32] by the interpolation equation of state for water of [48]. The intersection of the calculated adiabatic curve for a two-phase mixture [32] with the melting curve corresponded to a pressure of ~10 GPa. In so doing, the increase in the content of ice VII in the mixture as a result of the pressure increase from ~3 to 10 GPa corresponded to the values of α from zero to 0.25, i.e., to a partial formation of ice VII in the entire region below the melting curve.

Given in the *P–V* diagram in Fig. 5 are shock adiabatic curves for water [29, 35] (curves *7* and *6*); its isentrope by the data of [29], which corresponds to the temperature variation from 340 to 440 K (curve *5*); and the isotherm for water T_0 = 573 K by the data of [49], which was obtained using the data of [20] (curve *4*). Figure 5 further gives, for ice VII, the isotherms T = 300 and 600 K [37] (curves *1* and *2*) and the dependence $V(P)$ on the melting curve [37] (curve *3*). Dotted curves *8–10* are shock adiabatic curves for ice VII, two-phase mixture, and water at pressures up to 10 GPa by the data of [32]. The adiabatic curve for the two-phase mixture is fairly close to the experimental data of [29] and corresponds to the temperature variation from 350 to 570 K. The hypothetical calculated shock adiabatic curves for ice VII and water [32], which correspond to approximately the same temperature range, differ from the respective calculated and experimentally obtained isotherms and isentrope for water. For the shock adiabatic curve of ice VII, this difference is associated, in particular, with the fact that the initial density of ice was taken to be 1.52 g/cm^3, i.e., Rybakov and Rybakov [32] actually treated ice VII as a low-compressible addition to water. Nevertheless, it follows from the foregoing data that the transition to the liquid state region on the shock adiabatic curve for water occurs at a pressure which exceeds approximately 13-15 GPa. Below this pressure, the shock compression of water in the range $2.4 < P <$ 13–15 GPa may correspond to the state of two-phase mixture of ice VII and water with prevailing content of water.

If we proceed from the assumption of the relaxation pattern of phase transformation of water to ice VII, the formation of a mixture of phases under shock compression explains partly the data on the transparence of water behind the shock front and the dispersion of ice VII being formed [20, 23, 33, 34]. However, in view of the simplifications adopted in [32] for the equations of state for water and ice VII, the obtained results must be treated as rather approximate. The kinetic mechanism of the process of formation of ice VII under shock compression is not yet known. As was demonstrated by Chizhov [50], the kinetics of phase transitions of ice I–VII and of their melting play an important part under conditions of shock loading of ice I.

DETERMINING THE VISCOSITY BY THE METHOD OF HARMONIC PERTURBATIONS

The method of investigation of shear viscosity of matter behind the shock front [1] was suggested by Academician A.D. Sakharov and associates in 1957 [51]. The method is based on studying the time evolution of small harmonic perturbations developed on the front of a shock wave propagating in the material being investigated, with subsequent comparison of the experimental results with theory. The experimental investigations were performed at VNIIEF (All-Russia

Research Institute of Experimental Physics) in Sarov by Mineev, Oleinik and others [1, 5, 6, 52]; the results were numerically processed by Zaidel' [53] who treated the effect of viscosity on the development of perturbations in a plane shock wave.

Somewhat later, Miller and Ahrens [54] analyzed in more detail the method of determining viscosity, which was suggested in [1], and treated the effect of boundary conditions and approximations adopted in [53] on the results of experimental determination of the viscosity of water in [5, 6]. Similarly to Zaidel' [53], Miller and Ahrens [54] solved the problem on the propagation of perturbations using the approximation of Newtonian fluid of constant viscosity which is independent of the rate of loading. Comparison of the estimates of viscosity of water [5, 6] using two approaches [53, 54] revealed a slight difference between the results, which supported the validity of the data obtained in [1, 5, 6, 52].

In the experiments, a plane shock wave in the material under investigation, namely, water placed in a thin-walled cuvette, was developed using an explosive charge in which a plane detonation wave was initiated. In order to provide harmonic perturbations on the shock front in water, use was made of a paraffin disk (with recesses in the form of parallel cavities of sinusoidal profiles) placed between the charge and material under investigation. Harmonic perturbations on the shock wave appeared when the shock wave arrived at the front surface of the cuvette. The distance between the cavities defined the length of the perturbation wave on the shock front. For recording the development of perturbations at different instants of time during one experiment, a wedge-shaped cuvette was used. The profile of the shock wave front after its propagation in the sample was measured by the glow in the gap between the rear surface of the cuvette and a transparent (Plexiglas) plate. The glow was recorded by a super-high-speed streak camera. A system of slits provided on the plate was used as a light screen for recording the wave profile at different instants of time corresponding to the path of shock wave propagation on the wedge.

Because the shock adiabatic curve for paraffin is close to that for water [55, 56], no special calculation was performed of the propagation of perturbation in view of the paraffin layer. Check experiments, in which paraffin was replaced by lead (with the same shock wave pressure in water), revealed that the development of perturbations in both cases coincides within the experimental error [5].

The viscosity was measured in the pressure range from 4 to 25 GPa corresponding to the density of water from 1.45 to 1.98 g/cm^3 [5, 6]. The pressure increase in the shock wave to 25 GPa in [6] was attained owing to the use of a laboratory explosive device employed at VNIIEF to investigate the shock compression of matter with the acceleration of a steel envelope by explosion products [57].

Artificially produced perturbations, which are characterized by periodicity in the direction along the shock front, set the material behind the front in vibrational motion. The perturbation parameters were selected such as to satisfy the approximation [53] corresponding to plastic flow disregarding the strength and effect of low viscosity on the development of perturbations,

$$Pa_0/\lambda > \sigma_p, \quad 2\pi a_0/\lambda << 1. \qquad (4)$$

Here, a_0 is the initial amplitude of perturbations, λ is the perturbation wavelength, P is the shock wave pressure, and σ_p is the dynamic ultimate strength [58, 59]. The constancy of flow behind the shock front for different wavelengths, which is necessary for agreement between the theory and experiment, was provided by the use of fairly large-size explosive charges and assemblies with cuvettes.

The perturbed flow of matter on the shock front, which corresponds to high-rate strain, is characterized by the relations for strain and rate of strain [52],

$$\varepsilon = 2\pi a_0/\lambda, \quad d\varepsilon/dt = 4\pi^2 a_0 D/\lambda^2. \qquad (5)$$

In the experiments, the strain was ε = 20 to 140 %, and $d\varepsilon/dt = (1–6)\times10^5$ s^{-1}.

The propagation of shock waves with different perturbation wavelengths λ on the front was studied. In the experiments, complete geometric modeling was performed of the process under similar conditions differing in scale, including the validity of the relation $2\pi a_0/\lambda$ = const.

The amplitudes of perturbations on the shock front were measured for wavelengths λ = 1 and 2 cm and initial amplitudes $2\pi a_0/\lambda$ = 0.19–1.13. Figure 6 gives typical experimental data on the development of perturbations on the shock front depending on the reduced path of shock wave propagation $x = s/\lambda$ (s is the path covered by the wave) [52]. The pattern of experimentally obtained curves was qualitatively the

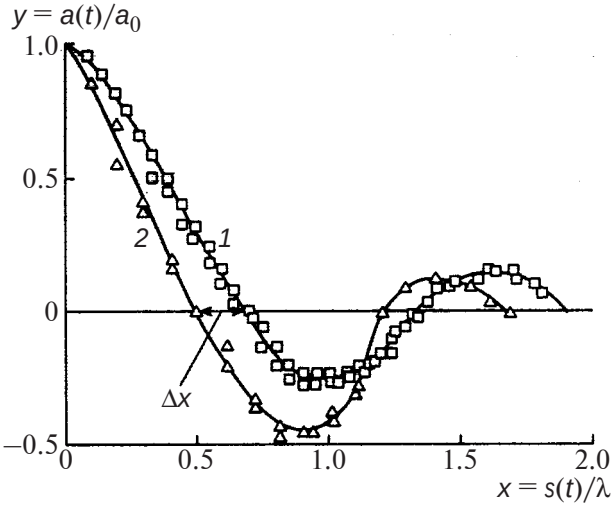

Fig. 6. Experimentally obtained curves of the development of the reduced amplitude of perturbations on the shock front according to the data of [52]: (*1*) λ = 2 cm, $2\pi a_0/\lambda$ = 0.872; (*2*) λ = 1 cm, $2\pi a_0/\lambda$ = 0.872; Δx, phase shift.

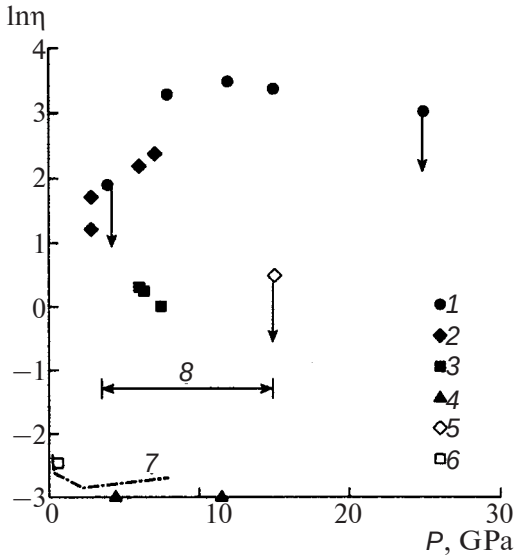

Fig. 7. The viscosity–shock-compression pressure diagram for water, η in Pa s: (*1*) data of [5, 6], (*2*) data of [7], (*3*) data of [8], (*4*) data of [19], (*5*) data of [63], (*6*) data of [64], (*7*) pressure dependence of viscosity on the melting curve [16], (*8*) region of two-phase state.

same as in the calculation of Zaidel' [53]: the perturbation amplitude decayed while changing sign several times. At the same time, it was found that the curves of decay of perturbation amplitude $a(x)/a_0$ for different values of wavelength λ and parameter $2\pi a_0/\lambda$ in coordinates x were phase shifted. Analysis of the calculation results revealed that the phase shift in the case of complete geometric modeling is possible due to viscosity, i.e., is determining for the value of shear viscosity which may be calculated by the shift $\Delta x = x_{02} - x_{01}$ of the intersection between the a/a_0 curve and abscissa for different wavelengths,

$$\eta = \rho D \Delta x / k(1/\lambda_1 - 1/\lambda_2), \qquad (6)$$

where ρ is the density behind the unperturbed shock front, and D is the wave velocity of this front. The parameter k was found from regression analysis of data $x_{0i} = f(1/\lambda_i, a_{0i}/\lambda_i)$ given in [1]. The obtained curves of variation of perturbation amplitude on the shock front from the reduced path for water were similar to those of dependences measured for metals previously investigated in [1, 52].

Figure 7 gives the results of determination of the viscosity of water as a function of pressure on the shock adiabatic curve. The results of measurements in the pressure range from 3 to 15 GPa lie below the melting curve and correspond to the two-phase state in the temperature range from 400 to 700 K (see Fig. 4). When the pressure varies from 4 to 8 GPa, the viscosity of shock-compressed water increases by more than an order of magnitude, which is possibly associated with the increase in the fraction of ice VII being formed; after that, the viscosity remains approximately constant and equal to ~2–3 kPa s. With the pressure P = 25 GPa and shock compression temperature ~1800 K [28], the viscosity decreases and corresponds to that in the liquid state. Because the limiting possibilities of recording the development of perturbations amounted to $\Delta x \sim 0.02$–0.03, the viscosity determined at P = 4 and 25 GPa agreed with the estimates of $\eta <$ < 0.08 kPa s and $\eta <$ 1 kPa s.

With a pressure of ~10 GPa, the viscosity of ~1 kPa s turned out to be close to values corresponding to solid state on the shock-compression adiabatic curves [1, 52] obtained for aluminum and lead at pressures P = 30–40 GPa. The maximal values of viscosity of metals were approximately three to five times those for water. These states corresponded to approximately the same strains and strain rates ε and $\dot{\varepsilon}$. In the region above the melting curve for metals, similarly to the case for water, data were obtained which corresponded to the limiting possibilities of recording the development of perturbations and were indicative of significant decrease in viscosity compared to the maximal values.

VISCOSITY MEASUREMENTS USING THE METHODS OF ACCELERATION OF A BODY AND OF ELECTRICAL CONDUCTIVITY

In a series of studies [7–9], Al'tshuler, Kanel', Kim, and others suggested a method of measuring the viscosity by recording the velocity of a cylindrical body (wire) accelerated by a flow behind the front of a plane shock wave (method of accelerating cylinders) and obtained data on the viscosity of water and other liquids. Note that the detailed checking of the method performed by Kim [8] revealed that the initial unsteady stage of flow past a wire, which introduces errors into the measurement results, is defined by the wire diameter, and the gage length for velocity measurements must significantly exceed the initial acceleration process. The diameter of metal wires under the experimental conditions must not exceed ~0.04 mm. Even in the first measurements [7], wire sensors were used whose diameter was approximately an order larger; because of this, Kim [8] and Al'tshuler *et al.* [9] assumed that the data of [7] were inaccurate. Moreover, the measurements of water viscosity [7–9] were performed in a relatively narrow pressure range of 6–7 GPa corresponding to the two-phase state on the shock adiabatic curve. As was observed by Miller and Ahrens [54], the presence of fine crystalline ice behind the shock front must lead to a variation of the dependence of the cylinder acceleration on viscosity. When the wire diameter decreases to a size close to that of ice crystals, the effect of the latter on the wire in the flow behind the shock front decreases, and the wire acceleration is largely defined only by the viscosity of the liquid component of the mixture. Therefore, the results of measurements of viscosity in this pressure range appear to be incorrect, in contrast to the data of measurements performed for glycerin in a single-phase region [9].

Another group of data on the viscosity of water were obtained by Hamann and Linton [19, 60] as a result of measurements of impurity electrical conductivity Σ of aqueous electrolytic solutions under shock compression. The viscosity at pressures P = 4.5 and 11 GPa was calculated by the Walden relation ($\eta\Sigma$ = = const) [61] whose validity is called into question [6, 9] because of the difference between the mechanisms and factors defining the ion mobility and the structural viscosity of water at high pressures and densities realized under shock compression. In addition, according to estimates of Hamann and Linton [19], the measured electrical conductivity at a pressure of 11 GPa corresponds to the dissociation of 0.5% of water molecules. The electrical conductivity measured in [19] fitted well the dependence obtained by Mitchell and Nellis [27] for pure water[2]. As was observed by Miller and Ahrens [54], the same electrical conductivity corresponds to the dissociation of free water in the water–ice VII two-phase mixture; however, its viscosity must increase significantly because of the presence of fine crystalline ice.

Indirect estimates of the viscosity of water [63], made by the rate of coagulation of sulfur particles in solutions of sodium thiosulfate at a shock compression pressure P = 15 GPa, gave a value of $\eta \le 3$ Pa s which does not contradict the concept of viscosity decrease in the region above the melting curve. However, this value may also be referred to the viscosity of the liquid component of the mixture.

The shock compression of water in the pressure range $P < 2.4$ GPa does not cause a variation of its initial aggregate state corresponding to the values of viscosity obtained in static measurements. In accordance with the data of Lyusternik [16], the viscosity of water on the solidification curve corresponds to the minimal value at the water–ice VI–ice VII triple point at a pressure of 2.2 GPa (Fig. 1). The results of measurements of the coefficient of reflection of light from the shock front performed by Harris and Presles [64] at a pressure of 0.58 GPa made it possible to estimate the viscosity at the front: $\eta \le 60$ mPa s. The parameters of this state are close to those of the ice V–ice VI triple point on the melting curve, to which the viscosity η = 2.2 mPa s corresponds [16].

Figure 7 gives the available data on the viscosity of water under shock compression [5–9, 19, 63, 64], as well as those on the melting curve for ice VII [16]. A major part of the data were obtained in the water–ice VII two-phase region.

CONCLUSIONS

Previous analysis of the results of viscosity measurements [5, 6], which is largely based on the data of [20, 22, 35], partly coincides with the interpretation given by us and proceeding from the fact that ice VII forms as a result of shock compression of water. The existence of the water–ice VII two-phase state on the shock adiabatic curve was previously admitted in a

[2]The first measurements of electrical conductivity of shock-compressed water at a pressure P = 10 GPa were performed by Brish *et al.* [62].

limited region on the melting curve [6]. The refinement of the phase diagram for water using the experimental data obtained after the publication of the results of [5, 6] and the theoretical estimates of states on the shock adiabatic curve in [3, 16, 32, 37] and in other studies made possible a new explanation of the available experimental results on viscosity under shock compression.

In the entire pressure range below the melting curve after the first intersection of this curve with the shock adiabatic curve corresponding to the range from 4 to 15 GPa, the increase in viscosity is associated with a gradual increase in the fraction of ice VII in the two-phase mixture. According to the data of [5, 6], the viscosity of water in the pressure range of 12–15 GPa remains high, $\eta \simeq 2$–3 kPa s. This is confirmed by Miller and Ahrens [54] who performed a more detailed processing of the results of measurements of [5] at a pressure $P = 15$ GPa, which gave a value of $\eta = 2.0$ kPa s close to the value of $\eta = 2.2$ kPa s obtained in [5]. A further increase in the shock compression pressure leads to a transition to the liquid state and to an increase in viscosity.

Miller and Ahrens [54] pointed to the possibility of the local heterogeneous two-phase state under shock compression of water affecting the results of viscosity measurements obtained by the method of acceleration of a wire sensor, as well as the results of measurements of electrical conductivity which were used to estimate the viscosity using the Walden relation. These measurements were largely associated with the viscosity and electrical conductivity of the liquid component of the water–ice VII two-phase state, which resulted in a reduction of the values of viscosity obtained in [7–10].

REFERENCES

1. Sakharov, A.D., Zaidel', R.M., Mineev, V.N., and Oleinik, A.G., *Dokl. Akad. Nauk SSSR*, 1964, vol. 159, no. 5, p. 1019.
2. Först, P., Werner, F., and Delgano, A., *Rheol. Acta*, 2000, vol. 39, p. 566.
3. Nagayama, K., Mori, Y., Shimada, K., and Nakahara, M., *Water Shock Hugoniot Measurement up to Less than 1 GPa, in Shock Compression of Condensed Matter–1999. Proc. Am. Phys. Soc.*, Furnish, M.D., Chhabildas, L.S., and Hixson, R.S., Eds., Amsterdam: Elsevier, 2000, p. 65.
4. Altshuler, L.V., Viscosity of Water and Glycerin behind a Shock Wave Front, in *Shock Compression of Condensed Matter–1991. Proc. Am. Phys. Soc.*, Schmidt, D.T. *et al.*, Eds., Amsterdam: Elsevier, 1992, p. 509.
5. Mineev, V.N. and Zaidel', R.M., *Zh. Eksp. Teor. Fiz.*, 1968, vol. 54, no. 6, p. 1633.
6. Mineev, V.N. and Savinov, E.V., *Zh. Eksp. Teor. Fiz.*, 1975, vol. 68, no. 4, p. 1321.
7. Al'tshuler, L.V., Kanel', G.I., and Chekin, B.S., *Zh. Eksp. Teor. Fiz.*, 1977, vol. 72, no. 2, p. 663.
8. Kim, G.H., *Prikl. Mekh. Tekh. Fiz.*, 1984, no. 5, p. 44.
9. Al'tshuler, L.V., Doronin, G.S. and Kim, G.H., *Prikl. Mekh. Tekh. Fiz.*, 1986, no. 6, p. 110.
10. Nabatov, S.S., Shunin, V.M., and Yakushev, V.V., The Viscosity of Liquid Inert and Explosive Matter behind the Shock Front, in *Khimicheskaya fizika protsessov Goreniya i Vzryva. Detonatsiya* (Chemical Physics of Processes of Combustion and Explosion: Detonation), Chernogolovka: Izd. OIKhF AN SSSR (Division of Inst. of Chemical Physics, USSR Acad. Sci.), 1977, p. 116.
11. Bridgman, P.W., *Proc. Am. Acad. Arts Sci*, 1926, vol. 61, p. 57.
12. Bett, K.E. and Cappi, J.B., *Nature*, 1965, vol. 207, p. 620.
13. DeFries, T. and Jonas, J., *J. Chem. Phys.*, 1977, vol. 66, p. 896.
14. Jonas, J., DeFrries, T., and Wilbur, D. J., *J. Chem. Phys.*, 1976, vol. 65, p. 582.
15. Dougherty, R.C. and Howard, L.N., *J. Chem. Phys.*, 1998, vol. 109, no. 17, p. 7379.
16. Lyusternik, V.E., *Teplofiz. Vys. Temp.*, 1990, vol. 28, no. 4, p. 686.
17. Hirschfelder, J.O., Curtiss, C.F., and Bird, R.B., *Molecular Theory of Gases and Liquids*, New York: Wiley, 1954. Translated under the title *Molekulyarnaya teoriya gazov i zhidkostei*, Moscow: Izd. Inostrannaya Literatura, 1961.
18. Al'tshuler, L.V., *Usp. Fiz. Nauk*, 1965, vol. 85, no. 2, p. 197.
19. Hamann, S.D. and Linton, M., *J. Appl. Phys.*, 1969, vol. 40, p. 913.
20. Walsh, J.M. and Rice, M.H., *J. Chem. Phys.*, 1957, vol. 26, no. 4, p. 815.
21. Al'tshuler, L.V., Bakanova, A.A., Trunin, R.F., *Dokl. Akad. Nauk SSSR*, 1958, vol. 121, no. 1, p. 67.
22. Schroeder, R.C. and McMaster, W.H., *J. Appl. Phys.*, 1973, vol. 44, no. 6, p. 2591.
23. Kormer, S.B., Yushko, K.B., and Krishkevich, G.V., *Zh. Eksp. Teor. Fiz.*, 1968, vol. 54, no. 6, p. 1640.
24. Skidmore, I.C. and Morris, E., Experimental Equation of State Data for Uranium and Its Interpretation in the Critical Region, in *Proceedings of a Symposium*, Vienna, 1962, p. 173.
25. Volkov, L.P., Voloshin, N.P., Mangasarov, R.A. *et al.*, *Pis'ma Zh. Eksp. Teor. Fiz.*, 1980, vol. 31, no. 9, p. 546.
26. *LASL Shock Wave Hugoniot Data*, March, S.P., Ed., Berkeley: University of California Press, 1980.
27. Mitchell, A.C. and Nellis, W.J., *J. Chem. Phys.*, 1982, vol. 76, no. 12, p. 6273.
28. *Eksperimental'nye dannye po udarno-volnovomu szhatiyu i adiabaticheskomu rashireniyu kondensirovannykh veshchestv* (Experimental Data on Shock-Wave Compression and Adiabatic Expansion of Condensed Matter), Trunin, R.F.,

Ed., Sarov: RFYaTs–VNIIEF (Russian Federal Nuclear Center–All-Russia Research Inst. of Experimental Physics), 2001.

29. Bakanova, A.A., Zubarev, V.N., Sutulov, Yu.N., and Trunin, R.F., *Zh. Eksp. Teor. Fiz.*, 1975, vol. 68, no. 3, p. 1099.
30. Sharipdzhanov, V.V., Al'tshuler, L.V., and Brusnikin, S.E., *Fiz. Goreniya Vzryva*, 1983, no. 5, p. 149.
31. Bogdanov, G.E. and Rybakov, A.P., *Prikl. Mekh. Tekh. Fiz.*, 1992, no. 2, p. 23.
32. Rybakov, A.P. and Rybakov, I.A., *Eur. J. Mech. B*, 1995, vol. 14, no. 3, p. 323.
33. Zel'dovich, Ya.B., Kormer, S.B., Sinitsyn, M.V., and Yushko, K.B., *Dokl. Akad. Nauk SSSR*, 1961, vol. 138, no. 6, p. 1333.
34. Kormer, S.B., *Usp. Fiz. Nauk*, 1968, vol. 94, no. 4, p. 641.
35. Rice, M.H. and Walsh, J.M., *J. Chem. Phys.*, 1957, vol. 26, no. 4, p. 824.
36. Pistorius, C.W.F.T., Pistorius, M.C., Blakeley, J.P., and Admiraal, L.J., *J. Chem. Phys.*, 1963, vol. 38, no. 3, p. 600.
37. Fei, Y., Mao, H., and Hemley, R.J., *J. Chem. Phys.*, 1993, vol. 99, no. 7, p. 5369.
38. Cowpertwaite, M. and Shaw, R., *J. Chem. Phys.*, 1970, vol. 53, no. 2, p. 555.
39. Kwai, N. and Inokuti, Y., *Jpn. J. Appl. Phys.*, 1970, vol. 9, no. 1, p. 31.
40. Gurtman, G.A., Kirschand, J.W., and Hasting, C.R., *J. Appl. Phys.*, 1971, vol. 42, no. 2, p. 851.
41. Lyzenga, G.A., Ahrens, T.J., Nellis, W.J., and Mitchell, A.C., *J. Chem. Phys.*, 1982, vol. 76, no. 12, p. 6282.
42. Ree, F.H., *J. Chem. Phys.*, 1982, vol. 76, no. 12, p. 6287.
43. Zharkov, V.N. and Trubitsyn, V.P., *Fizika planetarnykh nedr* (The Physics of Planetary Interior), Moscow: Nauka, 1980.
44. Ubbelohde, A., *Melting and Crystal Structure*, Oxford: Clarendon, 1965. Translated under the title *Plavlenie i kristallicheskaya struktura*, Moscow: Mir, 1969.
45. Impey, R.W., Klein, M.L., and McDonald, I.R., *J. Chem. Phys.*, 1981, vol. 74, no. 1, p. 647.
46. Olinger, B. and Halleck, P.M., *J. Chem. Phys.*, 1975, vol. 62, no. 1, p. 94.
47. Hemley, R.J., Jephcot, A.P., Mao, H.K. *et al.*, *Nature* 1987, vol. 330, no. 6150, p. 737.
48. Zamyshlyaev, B.V. and Menzhulin, M.G., *Prikl. Mekh. Tekh. Fiz.*, 1971, no. 3, p. 113.
49. Halbach, H. and Chatterjee, N.D., *Contrib. Mineral. Petrol.*, 1982, vol. 79, no. 3, p. 337.
50. Chizhov, V.E., *Prikl. Mekh. Tekh. Fiz.*, 1995, vol. 36, no. 6, p. 158.
51. Al'tshuler, L.V., Trunin, R.F., Urlin, V.D. *et al.*, *Usp. Fiz. Nauk*, 1999, vol. 169, no. 3, p. 323.
52. Mineev, V.N. and Savinov, E.V., *Zh. Eksp. Teor. Fiz.*, 1967, vol. 52, no. 3, p. 629.
53. Zaidel', R.M., *Prikl. Mekh. Tekh. Fiz.*, 1967, no. 4, p. 30.
54. Miller, G.H. and Ahrens, T.J., *Rev. Mod. Phys.*, 1991, vol. 63, no. 4, p. 919.
55. Al'tshuler, L.V. and Petrunin, A.P., *Zh. Eksp. Teor. Fiz.*, 1961, vol. 31, no. 6, p. 717.
56. Alekseev, Yu.F., Al'tshuler, L.V., and Krupnikova, V.P., *Prikl. Mekh. Tekh. Fiz.*, 1971, no. 4, p. 152.
57. Al'tshuler, L.V., Trunin, R.F., Krupnikov, K.K., and Panov, V.N., *Usp. Fiz. Nauk*, 1996, vol. 166, no. 5, p. 575.
58. Bogach, A.A. and Utkin, A.V., *Prikl. Mekh. Tekh. Fiz.*, 2000, vol. 41, no. 4, p. 198.
59. Rybakov, A.P., *Int. J. Impact Eng.*, 2000, vol. 24, p. 1041.
60. Hamann, S.D. and Linton, M., *Trans. Faraday Soc.*, 1969, vol. 65, no. 8, p. 2186.
61. Glasstone, S., Laidler, K.J., and Eyring, H., *Theory of Rate Processes*, New York: McGraw-Hill, 1941. Translated under the title *Teoriya absolyutnykh skorostei reaktsii*, Moscow: Izd. Inostrannaya Literatura, 1948.
62. Brish, A.A., Tarasov, M.S., and Tsukerman, V.A., *Zh. Eksp. Teor. Fiz.*, 1960, vol. 38, p. 22.
63. Yakusheva, O.B., Yakushev, V.V., and Dremin, A.N., The Formation of Sulfur Particles in Sodium Thiosulfate Solutions behind the Shock Front, in *Materialy III Vsesoyuznogo simpoziuma po goreniyu i vzryvu* (Proceedings of III All-Union Symposium on Combustion and Explosion), Moscow: Nauka, 1972, p. 544.
64. Harris, P. and Presles, H.N., *J. Chem. Phys.*, 1981, vol. 74, no. 12, p. 6864.